PCCP

The halogen effect on the ^{13}C NMR chemical shift in substituted benzenes

Journal:	*Physical Chemistry Chemical Physics*
Manuscript ID	CP-ART-02-2018-001249.R1
Article Type:	Paper
Date Submitted by the Author:	28-Mar-2018

Complete List of Authors:	Vidal Viesser, Renan; University of Campinas, Institute of Chemistry Ducati, Lucas; University of Sao Paulo, Department of Fundamental Chemistry Tormena, Claudio; State University of Campinas, Chemistry Institute Autschbach, Jochen; University at Buffalo, State University of New York, Chemistry

The halogen effect on the ^{13}C NMR chemical shift in substituted benzenes

Renan V. Viesser,[a] Lucas C. Ducati,[b*] Cláudio F. Tormena,[a*] Jochen Autschbach[c*]
[a] Institute of Chemistry, University of Campinas - UNICAMP
P. O. Box 6154, 13083-970, Campinas, SP, Brazil
*email: tormena@iqm.unicamp.br
[b] Department of Fundamental Chemistry
Institute of Chemistry, University of São Paulo
Av. Prof. Lineu Prestes, 748
05508-000, São Paulo, SP, Brazil
*email: ducati@iq.usp.br
[c] Department of Chemistry
University at Buffalo, State University of New York
Buffalo, NY 14260-3000, USA
*email: jochena@buffalo.edu

Abstract: Recent research [*Chem. Sci.*, 2017, **8**, 6570-6576] showed for R-substituted benzenes with R = NH_2, NO_2 that the substitution effects on the ^{13}C NMR chemical shifts are correlated with changes in the σ-bonding framework and do not follow directly the electron-donating or -withdrawing effects on the π orbitals. In the present work we extend the study to halogen (X = F, Cl, Br or I) substituted R-benzenes. The effect of X and R groups on ^{13}C NMR chemical shifts in X-R-benzenes are investigated by density functional calculations and localized molecular orbital analyses. Deshielding effects caused by the X atom on the directly bonded carbon nucleus are observed for F and Cl derivatives due to a paramagnetic coupling between occupied π orbitals and unoccupied $\sigma^*_{C\text{-}X}$ antibonding orbitals. The SO coupling plays an important role in the carbon magnetic shielding of Br and I derivatives, as is well known, and the nature of X also modulates the ^{13}C paramagnetic shielding contributions. Overall, the X and R substituent effects are approximately additive.

Keywords: NMR, shielding tensor, substituent effect, localized molecular orbitals, density functional theory

1 Introduction

The NMR chemical shift δ is an important property that provides a wealth of information about molecular structure and chemical bonding. The shift δ is a relative measure of the shielding constant σ for a nuclear isotope in a reference (ref) versus a probe environment, namely $\delta = \sigma_{ref} - \sigma$. This expression is usually an excellent approximation; when the reference shielding becomes very large the shielding difference must be divided by $1 - \sigma_{ref}$ in order to obtain the chemical shift. An increased δ, i.e. resonance at higher frequency, is associated with a less positive / more negative shielding, and *vice versa*. Older terminology, now deprecated, associates a more

positive / negative shielding with a higher / lower magnetic field needed to achieve resonance at a given frequency.

The chemical shift, and – more fundamentally – the nuclear magnetic shielding σ, are sensitive to the electronic environment experienced by the nucleus. The nuclear magnetic shielding relates the external magnetic field $\boldsymbol{B}_0$ to the induced magnetic field $\boldsymbol{B}_\mathrm{I}$ generated at the nucleus of interest by the interaction of the external field with the electrons in the molecule, and the resulting local magnetic field $\boldsymbol{B}_\mathrm{loc}$ at the nucleus[1] as follows:

$$\boldsymbol{B}_\mathrm{loc} = \boldsymbol{B}_0 - \boldsymbol{B}_\mathrm{I} \quad ; \quad \boldsymbol{B}_\mathrm{I} = \boldsymbol{\sigma}\boldsymbol{B}_0 \quad ; \quad \boldsymbol{B}_\mathrm{loc} = (1 - \boldsymbol{\sigma})\boldsymbol{B}_0 \tag{1}$$

Here, $\boldsymbol{\sigma}$ is the nuclear shielding tensor. In terms of its principal components $\sigma_{ii}, i = 1, 2, 3$, the shielding constant is the isotropic average $(1/3)\sum_i \sigma_{ii}$. The sign conventions are chosen such that in most cases, when the shielding is positive, the induced field is counter-acting the external field. The fact that the NMR shielding is a tensor implies that it may not only influence the magnitude of the local field but also its direction relative to the external field. Accordingly, information about the electronic structure beyond that contained in the isotropic shielding is furnished by the relative signs and magnitudes of the principal components of $\boldsymbol{\sigma}$, and by the orientation of its principal axis system (PAS) relative to the molecular coordinate frame.[2]

^{13}C NMR chemical shifts in aromatic compounds are sensitive to substituent effects. In turn, substituents determine the chemical reactivity of the aromatic ring in electrophilic aromatic substitutions,[3–5] among other effects.[6,7] For instance, benzene ring substituents are classified as activating or deactivating towards electrophilic attack. An activating substituent such as $–NH_2$ increases the aryl electron density in certain positions, which then become preferred targets for electrophilic substitutions. A deactivating ligand such as $–NO_2$ has basically the opposite effect. The observed ^{13}C NMR shielding follows qualitatively the same trend, namely the shielding increases in the activated positions, relative to benzene, and decreases in the deactivated positions. A simple explanation for the shielding - reactivity correlation is that more electrons – i.e. a higher electron density – produce a stronger nuclear magnetic shielding and vice versa. However, the shielding is a response property, meaning that it depends not only on the bonding in the ground state but also on how the electronic system responds to the magnetic field. Therefore, the shielding is not in a simple direct way related to the electron density.

While the chemical substituent effects for aryl rings are associated with the π-bonding framework, we showed recently that the concomitant ^{13}C shielding effects are associated with the σ bonding framework.[8] Specifically, we evaluated how carbon shielding tensors in *ortho*, *meta*, and *para* positions are affected by the amino (NH_2) and nitro (NO_2) groups in aniline and nitrobenzene, respectively. Electron-donating and electron-withdrawing effects on the π system induce

opposite changes in the carbon σ-bond framework, and the ^{13}C substitutent effects on the NMR shielding and chemical shifts are determined solely by the occupied $\sigma_{C\text{-}C}$ and $\sigma_{C\text{-}H}$ localized molecular orbitals (LMOs) and their response to the magnetic field. We identified the magnetic coupling between occupied σ and unoccupied π^* orbitals (see Fig. 1) as the source of the paramagnetic component of the shielding that is sensitive to the effects caused by NH_2 and NO_2 substituents. The trends are then easily explained by an increase or decrease of the atomic orbital (AO) coefficients of the relevant LMOs at the carbon of interest, which is related to the electron density rearrangements in the σ-bonding framework. These density rearrangements are coupled in a mirror-image fashion to the same π-framework substituent effects that are responsible for the observed chemistry.

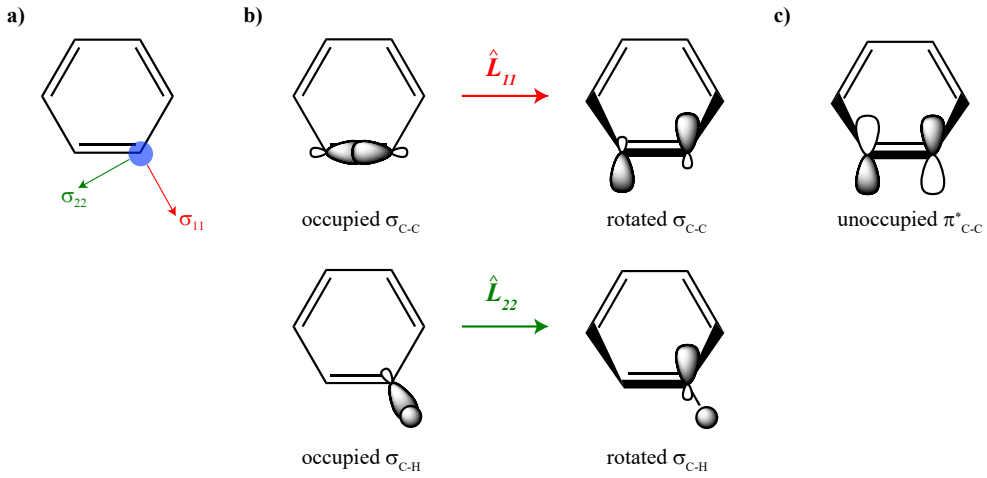

Figure 1: (a) Orientation of the principal shielding tensor components of the highlighted carbon atom. σ_{33} (not shown) is perpendicular to the aryl ring plane. (b) Occupied σ orbitals that may rotate under the action of an angular momentum operator ($\hat{L}$) and overlap after rotation with an unoccupied π^*_{C-C} orbital (c). The rotation - overlap picture indicates which orbitals couple magnetically under the action of a magnetic field in the 11 or 22 direction and give a contribution to the paramagnetic component of σ_{11} or σ_{22}. For more information see References 8 and 9, and Section 3.3 below.

Halogens (X = F, Cl, Br, I) are substituents that also cause strong and systematic effects on ^{13}C NMR chemical shifts in organic compounds, aromatic or not, especially on the shift of a carbon atom that is directly bound to X. These effects typically lead to one of two pronounced trends along the series F, Cl, Br, I: Normal Halogen Dependence (NHD) or Inverse Halogen Dependence (IHD). NHD refers to an increasing shielding (decreasing shift) with increasing halogen atomic number, while IHD refers to a reverse de-shielding trend.[10,11]

As the name implies, NHD is more commonly observed, in particular in organic compounds. NHD has a seemingly straightforward rationale, namely that the shielding increases along the se-

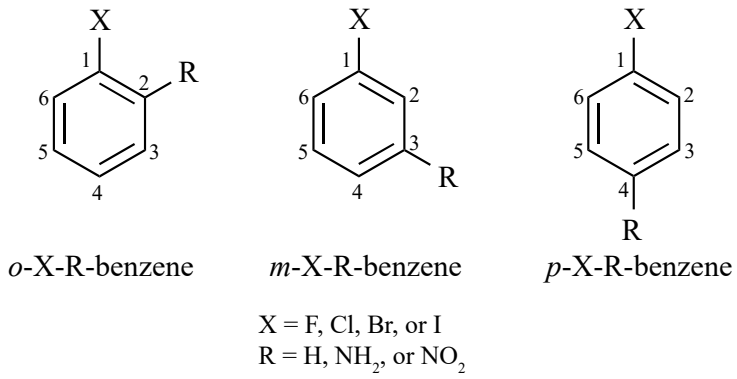

Figure 2: Structures and atom numbering of studied compounds.

ries F to I because the halogen electronegativity decreases, presumably leading to more electron density on the atom bound to it. However, this is another case where the electron density argument is much too simplistic. The true reason for NHD is a relativistic effect, spin-orbit (SO) coupling, that increases strongly with the halogen nuclear charge Z.[11–13] The SO coupling causes the external magnetic field to induce spin polarization at the halogen (and other heavy atoms), which is transmitted to another nucleus via covalent interactions. The magnetic field from the induced electron spin density may create a strong shielding effect particularly at the atom directly bound to the halogen.[14] Because of a very strong dependence on the atomic number, going in leading order[15] formally as $\sim Z^2$, this effect is most pronounced for bromine and especially iodine derivatives. IHD, on the other hand, is not primarily a relativistic effect but attributed to the paramagnetic current density induced by the magnetic field, via magnetic coupling of occupied and unoccupied orbitals similar to those shown in Figure 1. The inverse halogen trend is connected with the electronegativity effects on the energetic spacing between the ground state and excited states, and, like NHD, not simply related to the electron density. IHD is mainly observed in transition metal complexes.[12,13,16]

The haloanilines and halonitrobenzenes shown in Figure 2 were selected for the present study to evaluate the effects of halogen (X), and NH_2 and NO_2 substituents (R) on aryl ^{13}C chemical shifts, and to discern their origins. The carbon bound to the halogen (C1) is studied, to allow a simultaneous investigation of the SO coupling and how the relative positions *ortho*, *meta*, and *para* of the X and R groups affect the C1 shielding. The substituent effects on the C1 chemical shift were determined experimentally and analyzed theoretically. The calculated ^{13}C NMR shielding tensor ($\boldsymbol{\sigma}^{\text{total}}$) was partitioned into the usual diamagnetic ($\boldsymbol{\sigma}^{\text{dia}}$), paramagnetic ($\boldsymbol{\sigma}^{\text{para}}$), and spin-orbit ($\boldsymbol{\sigma}^{\text{SO}}$) contributions, using Kohn-Sham density functional theory (KS-DFT). The role of the σ and π bonds was rationalized via DFT-based analyses of $\boldsymbol{\sigma}^{\text{total}}$, and its dia, para, and SO contributions, in terms of Canonical Molecular Orbitals (CMOs, the 'usual' MOs), Natural Localized Molecular

Orbitals (NLMOs), and Natural Bond Orbitals (NBOs). Moreover, the effect of the magnetic field orientation relative to the molecule was introduced analyzing the principal components of $\boldsymbol{\sigma}^{\text{total}}$ in terms of a molecule-fixed principal axis system (PAS). Analyses of the shielding tensor in terms of 'chemist's orbitals' representing individual bonds, core shells, lone pairs, and antibonding orbitals are able to gain deep insight into how stereoelectronic interactions and relativistic effects influence the de(shielding) effects.

2 Experimental and computational details

^{13}C NMR spectra were recorded on a Bruker Avance III spectrometer operating at 600.17 MHz and 150.92 MHz for ^{1}H and ^{13}C, respectively. The samples were prepared as solutions of ca. 15 mg cm^{-3} in $CDCl_3$ or DMSO-d_6. The compounds were purchased from Sigma-Aldrich and used without further purification.

The calculations were performed with the Amsterdam Density Functional suite (ADF, version 2014).[17–19] Density functional theory (DFT) geometry optimizations and ^{13}C NMR shielding tensor calculations were performed with the PBE0[20] hybrid functional, and with TZ2P Slater-type orbital (STO) all-electron basis set from the ADF basis set library for all atoms. Benchmark calculations were performed with different functionals and basis sets, showing that the chosen level of theory is suitable for the purpose of this study – the additional results are collected in Section 2 of the Supplementary Information (SI). Becke integration grids[21] with the 'verygood' quality setting were selected for the numerical integrations, and the conductor-like screening model (COSMO)[22] with parameters for chloroform was applied to simulate (weak) solvent effects. Relativistic effects were included in the ground-state and NMR calculations via application of the two-component zeroth-order regular approximation (ZORA).[23–26] To improve the convergence of the hybrid DFT calculations, the input key 'AddDiffuseFit' was applied in order to generate additional density fit functions. The ^{13}C shielding tensors were calculated with the 'NMR' module of the ADF package, which utilizes the ZORA framework and the gauge-including atomic orbital (GIAO) distributed origin method. SO-specific self-consistent contributions from the DFT exchange-correlation response kernel (f_{XC}),[27–29] which are neglected by the version of the NMR program used for this study if default setting are applied, were included to improve the SO contributions to the shielding tensors for bromine and iodine derivatives.

The ^{13}C chemical shifts reported herein are referenced to tetramethylsilane (TMS). However, the chemical shifts δ_{i} were calculated with benzene as a secondary reference, via

$$\delta_{\text{i}} = \sigma_{\text{benz}} - \sigma_{\text{i}} + \delta_{\text{benz}} \tag{2}$$

Here, σ_{i} is the calculated shielding of the carbon nucleus of interest, and σ_{benz} and δ_{benz} are the calculated carbon shielding and the experimental chemical shift of benzene with respect to TMS, respectively. With exact calculated shielding tensors (including all influences from temperature, solvent, nuclear vibrations, etc.) there would be no difference between the result of Eq (2) and $\delta_{\mathrm{i}} = \sigma_{\mathrm{TMS}} - \sigma_{\mathrm{i}}$. The use of the secondary reference in the calculations improves the calculated chemical shifts by taking advantage of cancellation of errors. It is important to note, however, that the trends analyzed herein are not at all affected by the choice of the reference.

For each molecule, an NMR shielding analysis was carried out in terms of scalar relativistic (SR, i.e. calculated without SO coupling) localized molecular orbitals (LMOs), using the sets of 'natural' LMOs (NLMOs) and natural bond orbitals (NBOs) generated by the NBO 6.0 program[30] included with ADF. The analysis is described in more detail in References 31–34. The NLMO and NBO contributions of each NLMO to the principal components of the ^{13}C shielding tensor (σ_{11}, σ_{22}, and σ_{33}) were rationalized along the lines of References 31, 34. Due to the dependence of the NMR shielding on the local electronic structure around the nucleus of interest, analyses in terms of LMOs tend to be beneficial even though the apparently simple picture of magnetic coupling between unique pairs of canonical MOs (CMOs, the usual delocalized orbitals from self-consistent field calculations) is lost. There are as many doubly occupied SR NLMOs as there are doubly occupied SR CMOs, but there tend to be fewer NLMOs that have large contributions to the shielding of a given nucleus than CMOs.

For an analysis in terms of NLMOs, the shielding is expressed in terms of occupied CMOs, the occupied CMOs are transformed to the occupied NLMO basis, and the response to the external magnetic field is absorbed in the contributions from each occupied orbital. Each NLMO can in turn be expressed in terms of an ideally localized 'parent' NBO with a dominant coefficient in the expansion, plus a delocalization tail that is expressed in terms of the remaining NBOs. This leads to a shielding analysis in the basis of NBOs. The NBO set attempts to describe the molecule by an ideally localized set of bonding (BD), lone pair (LP) and core (CR) Lewis-type (L) orbitals, which may have occupation numbers of less than 2 for formally occupied, and greater than zero for formally unoccupied, orbitals in order to describe any non-Lewis (NL) contributions to the electronic structure. In the NLMO set, the L component is the parent NBO. If there is a NL component, it constitutes the 'delocalization tail' of the orbital and is given in terms of NBOs other than the parent. The shielding analysis can be partitioned accordingly into L and NL contributions, or per NBO individually. In either type of analysis, the response of the localized orbitals to the presence of the external magnetic field is absorbed into the shielding contributions, and the same occ-unocc pair of canonical MOs may contribute to several LMO shielding contributions.

The ADF NMR module uses the full set of SR LMOs (i.e. occupied and unoccupied) in order to analyze the shielding tensor calculated from a variational SO-ZORA calculation. For the closed-

shell molecules studied in this work, SO coupling does not strongly alter the ground state electronic structure. This leads in the analysis to comparatively minor contributions from LMOs that are not occupied in the SR ground state while the SO effects may show up, for instance, in a mixing of occupied σ and π two-center bonding LMOs. The shielding tensor can then be partitioned conveniently into Ramsey diamagnetic ('dia') and paramagnetic ('para') contributions, and an additional SO contribution. Any such partitioning is arbitrary but, as chosen, the dia and para contributions correspond closely to the ones known from the nonrelativistic theory of Ramsey and its SR analogs. Because of the variational character of the SO-ZORA ground state calculations, the dia and para contributions from SO-ZORA are not identical to those that would be obtained from SR-ZORA calculations, but they are close.

For the light nuclei in our samples, the SR effects on the NMR shieldings and chemical shifts are small. The SO effects generated at the heavy X substituents dominate the overall relativistic effects and are largely contained in the SO shielding contribution printed by the program. The para and SO contributions are not determined separately in the LMO analysis, because they both involve the response of the ground state to the presence of the external field, and because there are para-SO cross terms in the shielding tensor description.[31] In this work, the SO contributions are given as the difference of the sums para + SO from SO-ZORA calculations and the para contributions from separate SR-ZORA calculations. Consequently, σ^{para} is the paramagnetic shielding obtained from a SR-ZORA calculation, while σ^{SO} refers to the SO shielding contribution from a SO-ZORA calculation, as given by the program, plus minor SO effects on σ^{para}. The same partitioning was used for the shielding tensor principal components.

The Voronoi Deformation Density (VDD)[35–37] method was applied to calculate atomic charges and contributions to the deformation electron density of benzene upon R and X substitution. For the analysis, geometries were optimized in the gas phase assuming C_s symmetry to allow a VDD partitioning into A′ and A″ irreducible representations corresponding to the electronic rearrangements in the σ and π frameworks, respectively, relative to a promolecule composed of spherical atomic fragments. To analyze the charge rearrangements on the benzene ring caused by the R substituents, X-Ph$^{\bullet}$ and R$^{\bullet}$ radical fragments were generated using a KS restricted open-shell approach. Further information about the VDD procedure can be found in References 35 and 37.

3 Results and discussion

3.1 Overall trends for the isotropic chemical shifts

Per the numbering scheme of Figure 2, for consistency C1 is always the carbon for which the shielding is calculated and the positions *ortho*, *meta* and *para* are with respect to C1.

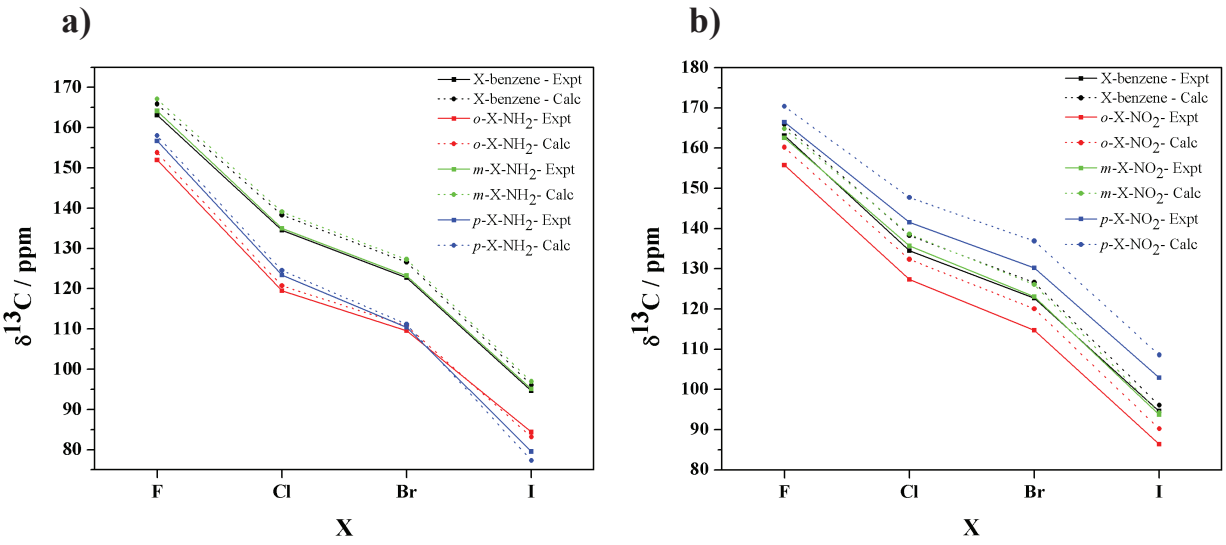

Figure 3: Calculated (Calc) and experimental (Expt) carbon 1 (C1, Figure 2) isotropic ^{13}C NMR chemical shifts for X-benzenes, X-NH_2-benzenes **(a)**, and X-NO_2-benzenes **(b)**. The calculated / experimental data are connected by dotted / solid lines in order to guide the eye.

Experimental ^{13}C NMR chemical shifts for the X-substituted carbon measured in a non-polar solvent ($CDCl_3$) and in a polar solvent (DMSO-d_6) are provided in Table S1 in the SI. The chemical shifts do not exhibit significant variations (∼1-2 ppm) due to the solvent polarity in most of the compounds. Moreover, the trends related to X effects and the position of the R groups do not change with solvent, indicating that observed experimental trends originate from intrinsic electronic effects in the molecular systems. The calculated ^{13}C NMR chemical shifts show good agreement with the experiments for all compounds, as displayed in Fig. 3. Importantly, the experimentally observed trends among the compounds are faithfully reproduced by the calculations, which means that a meaningful analysis of the trends can be carried out at the chosen level of theory.

As shown in Figure 3, there is a pronounced NHD (decreasing carbon shift) along the series X = F, Cl, Br, I, for all systems. We remind the reader that the NHD is mainly a SO relativistic effect associated with the increasing nuclear charge of the halogen. The NHD is overall more pronounced than the effects from the R substitutions; the range of the chemical shift reaches almost 80 ppm for the former and 17 ppm for the latter. Relative to X-benzene, the C1 nuclei (Fig. 2) experience a decreased chemical shift upon NH_2 substitution in *ortho* and *para* positions (Fig. 3a). This NH_2 group effect is larger for *ortho* than *para* when X = F, or Cl, very similar for both positions with X = Br, and larger for the iodine derivatives in *para* than *ortho* position. The effects from NO_2 substitution are overall less pronounced than for NH_2. Relative to X-benzene, the NO_2 substituent causes opposite effects for the C1 shift for the *ortho* and *para* isomers (Fig. 3b): The C1 shift

increases with NO_2 in the *para* position, while the shift decreases for the *ortho* isomer. In all cases, placing either one of the R substituents in the *meta* position has only a small effect on the C1 chemical shift.

In the following, we focus on the nuclear magnetic shielding rather than the chemical shift. To re-state the important trends in terms of shielding:

1. The NHD along the series X = F, Cl, Br, I produces an increased C1 shielding for increasing atomic number of X;

2. Relative to X-benzene and *meta*-substituted X-R-benzene, the NH_2 substituent causes increased shielding of C1 both in *ortho* and *para* positions;

3. Relative to X-benzene and *meta*-substituted X-R-benzene, the NO_2 substituent causes increased shielding of C1 in *ortho* and de-shielding in *para* position;

For the discussion, it is important to keep in mind that the terms paramagnetic and diamagnetic are used to partition the shielding into different mechanisms that contribute to the total, not the sign of observed trends. However, the diamagnetic shielding contribution is positive for carbon and tends to vary comparatively little among different compounds, while the paramagnetic contribution is usually negative and determines most of the magnitude and direction of the chemical shift at the SR level of theory. For our samples, the SO contribution to the C1 shielding is positive.

3.2 Trends for dia, para, and SO shielding contributions

Figure 4 shows the decomposition of the C1 isotropic NMR shielding constants into the diamagnetic (σ^{dia}), paramagnetic (σ^{para}), and SO (σ^{SO}) contributions. These results are displayed as a difference $\Delta\sigma$ relative to benzene, to allow an easier comparison. The corresponding numerical values are collected in Table S6 in the SI.

As expected, the largest variations are found for σ^{para} and σ^{SO}. The σ^{dia} contribution is affected mainly by the X group, which increases from X = F by up to about 10 ppm for Cl ≈ Br ≈ I (Figs. 4a and 4d). This is not an SO effect but present both in the SR and SO NMR calculations. The dia mechanism does not involve magnetic coupling of occupied and unoccupied orbitals and depends on the ground state electron density. Therefore, the increase of σ^{dia} from F to the other halogens is roughly consistent with the electronegativity trend in the X series. The R effects on σ^{dia} are smaller than 1 ppm and can be neglected completely. Despite some changes, σ^{dia} is not decisive for the observed trends overall. Accordingly the remaining discussion focuses on σ^{para} and σ^{SO}.

The C1 σ^{SO} contribution increases along the X series as it is expected for a relativistic effect, due to the increase of the nuclear charge of X. However, the observed increased shielding from

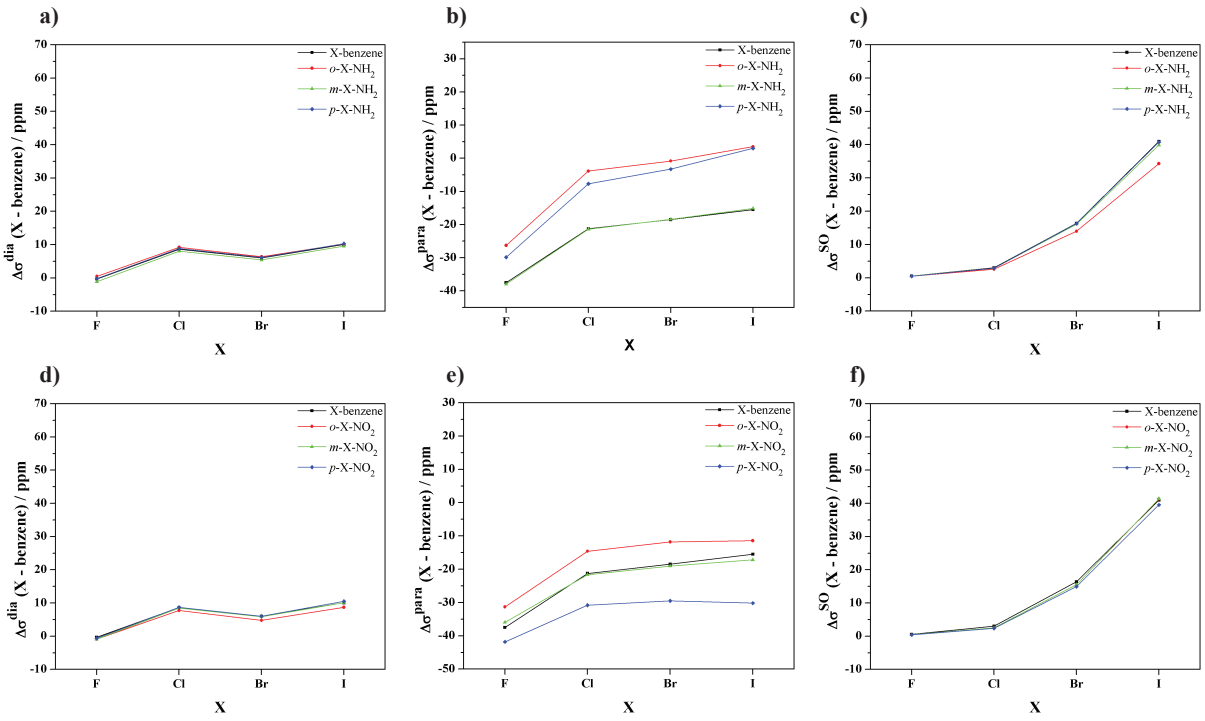

Figure 4: Decomposition of the C1 isotropic shielding into diamagnetic (first column = **a**, **d**), paramagnetic (second column = **b**, **e**), and SO (third column = **c**, **f**) contributions for X-R-benzenes. Top row: NH_2 substituent. Bottom row: NO_2 substituent. The shielding contributions are relative to benzene values:[8] σ^{dia} = 241.87 ppm, σ^{para} = -187.99 ppm, σ^{SO} = 0.76 ppm. Note that in each plot the scale of the vertical axis spans 80 ppm.

F to I with increasingly heavy X is caused by reinforcing paramagnetic and SO shielding contributions, with a positive change in σ^{para} being most important when going from F to Cl. The σ^{SO} contribution becomes dominant in the bromine and iodine compounds. The values of σ^{SO} are nearly the same for the different NO_2 substituent positions.

An interesting effect is observed for the *ortho* isomers of the NH_2 derivatives, namely that the SO contribution to the C1 shielding increases less pronouncedly from X = Cl to Br to I than it does when NH_2 is in the other two positions (Fig. 4c). This SO effect is accompanied by a decrease in the difference of σ^{para} for the *ortho* and *para* positions of NH_2 (Fig. 4b). These two trends combined lead to the reversal of the ^{13}C NMR chemical shift ordering between *ortho* and *para* isomers of X-NH_2-benzenes along the halogen series indicated by the crossing of the blue and red lines in Figure 3a.

The trends for the R substituents are in essence described by the σ^{para} contribution (Figs. 4b and 4e). For different positions of R, the trend lines along the X series have similar profiles, which suggest that the same electronic mechanisms are responsible for the variations of σ^{para} in the X-R-benzene systems. However, the magnitude of the carbon shift variations with the position of R is

sensitive to the nature of X. Furthermore, relative to benzene at 0 ppm, σ^{para} is strongly affected by the presence of a fluorine atom bonded to C1. Therefore, we can identify two trends in the X series: (i) σ^{para} strongly becomes more negative (25-40 ppm) going from benzene ('X' = H) to X = F; (ii) σ^{para} becomes less negative mainly from F to Cl (10-20 ppm), increasing slightly to more positive values (for R = NH_2) from X = Cl to I (5-10 ppm) or remaining relatively constant for the heavier halide ligands (for R = NO_2).

3.3 Analysis of the C1 nuclear magnetic shielding in terms of localized orbitals

As already mentioned, σ^{para} denotes the paramagnetic shielding obtained from SR-ZORA calculations, i.e., small SO effects affecting this contribution are not included in the analysis but absorbed in the SO contribution instead. In KS calculations, the paramagnetic term can be expanded into a 'sum-over-states' like expression, with CMO contributions for each of the tensor elements ($\sigma_{u,v}$ with $u, v \in \{x, y, z\}$) as[31]

$$\sigma_{u,v}^{para} = \text{const.}\ \text{Re} \sum_{i}^{\text{occ}} \sum_{a}^{\text{unocc}} \frac{\langle \varphi_i | \hat{F}_u^B | \varphi_a \rangle \langle \varphi_a | \hat{h}_v^\mu | \varphi_i \rangle}{\varepsilon_i - \varepsilon_a} \tag{3}$$

Here, φ_i, ε_i and φ_a, ε_a represent the occupied and unoccupied KS CMOs and their energies, respectively. The indices refer to linear perturbations by the nuclear spin magnetic moment (μ) and the magnetic field (B), and $\hat{F}$ and $\hat{h}$ are the KS Fock operator and its one-electron part. The two first-order perturbations of these operators essentially represent the relativistic analogs of the orbital Zeeman (OZ) and the electron spin-independent orbital paramagnetic (OP) hyperfine operator, respectively, and therefore, the paramagnetic component of the shielding tensor is given by the OZ-OP mechanism. $\hat{F}_u^B$ also includes the linear response of the KS potential to the external field perturbation, and in the calculations additional but relatively small contributions enter the OZ-OP mechanism from terms associated with the use of a finite GIAO basis. The SO shielding contribution has a somewhat similar expression as eq (3), but here the magnetic coupling is mainly involving orbitals with opposite spin projections. The reader is reminded that when the analysis is performed in terms of NLMOs (see Section 2), the summation over unoccupied orbitals is absorbed into the shielding contribution from each occupied NLMO. Similar considerations apply to the analysis in terms of NBOs.

Eq (3) indicates that the paramagnetic shielding terms are associated with magnetic interactions between occupied and unoccupied orbitals, and that they increase in magnitude with the increase of the OZ and OP interaction matrix elements in the numerator and a reduction of the

energy gaps between occupied and unoccupied orbitals in the denominator. Both the operators representing the external magnetic field $\boldsymbol{B}$ and nuclear magnetic moment $\boldsymbol{\mu}$ include an angular-momentum like operator, but the one for $\boldsymbol{\mu}$ strongly weighs the local electronic structure around the nucleus of interest. In order for a matrix element $\langle \text{unocc}|\hat{h}^{\mu}_{\upsilon}|\text{occ}\rangle$ to be large, one has to consider essentially the action of an angular momentum component υ on the part of the occupied orbital centered around the NMR nucleus, and whether the result has a large overlap with an unoccupied orbital, as sketched in Figure 1. Such a shielding contribution is particularly large if the two orbitals are close in energy.

The effect of an angular momentum operator component υ on atomic orbitals is effectively to produce zero for s orbitals and for p orbitals pointing in direction υ, and to rotate p orbitals that are perpendicular to υ by 90 degrees.[9,31,38] Similar results can be expected for atomic orbital contributions to the CMOs and LMOs around the nucleus of interest. After the rotation, a qualitative analysis can then focus on whether the locally rotated component of an occupied orbital overlaps well with parts of a low-energy unoccupied orbital. Such a finding would rationalize a substantial, usually negative, contribution to the paramagnetic shielding from the occupied orbital. This type of analysis for the paramagnetic shielding is sometimes aptly referred to as an 'orbital rotation model'.

For the SO contribution to the shielding, the orbital rotation model does not apply. Instead, the SO mechanism on the light nucleus in the vicinity of a heavy nucleus has a mechanism similar to that of $\boldsymbol{J}$-coupling,[11] which tends to be most effective when there is an easily spin-polarizable bond with substantial s character. The spin polarization is induced at the X site by the external magnetic field via the coupling of the electron spin to the orbital angular momentum. As for the para contribution, the SO mechanism tends to be more effective if the gaps between occupied and unoccupied orbitals are smaller, all else being equal.

The shielding tensor analysis is greatly simplified if it can be carried out in terms of the principal components σ_{ii} instead of the nine Cartesian components of eq (3). In this work, as already shown in Figure 1, the σ_{11} and σ_{22} components of the C1 shielding tensor lie in the aryl ring plane, while the most positive tensor component, σ_{33}, is perpendicular to the aryl ring plane.

The complete set of NLMO contributions for the C1 shielding are provided in Tables S7 - S15 in the SI. CR is short for core shells, LP for lone pair, and the other orbitals are labeled according to their parent NBOs. Halogen and oxygen LPs appear as an in-plane 2s-rich orbital ($LP_1(X)$), an in-plane 2p rich orbital ($LP_2(X)$), and a 2p-π LP perpendicular to the ring plane ($LP_3(X)$). The nitrogen LP of the NH_2 substituent is conjugated with the π system of the aryl moiety, and so are the π LPs of the NO_2 oxygens.

Several NLMOs give sizable contributions to σ^{para} and σ^{SO}. However, only a few orbitals dominate the X and R effects. The sum of $LP_1(X)$, $LP_3(X)$, $\sigma_{\text{C1-C2}}$, $\sigma_{\text{C1-C6}}$, $\sigma_{\text{C1-X}}$ and $\pi_{\text{C-C}}$ NLMO

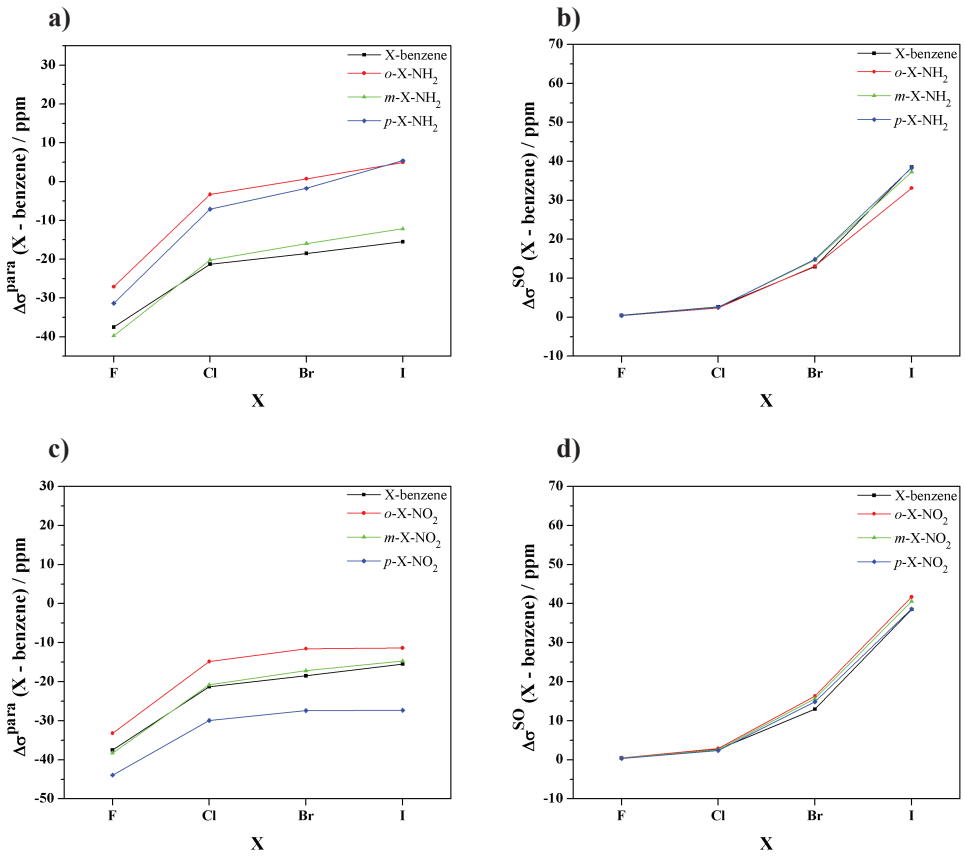

Figure 5: Sum of $LP_{1,3}(X)$, $\sigma_{C1\text{-}C,X}$ and $\pi_{C\text{-}C}$ NLMO contributions to the σ^{para} term (**a**, **c**), and sum of CR(C1), $LP_1(X)$, $\sigma_{C1\text{-}X}$, and $\sigma^*_{C1\text{-}X}$ NLMO contributions to the σ^{SO} term (**b**, **d**) of the C1 shielding for X-R-benzenes. Top row: NH_2 substituent. Bottom row: NO_2 substituent. The shielding contributions are relative to benzene values:[8] σ^{dia} = 241.87 ppm, σ^{para} = -187.99 ppm, σ^{SO} = 0.76 ppm. Note that in each plot the scale of the vertical axis spans 80 ppm.

contributions (Figure 5a and 5c) reproduces well the σ^{para} trends displayed in Figure 4. Likewise, the σ^{SO} trends are correctly described by the sum of only the CR(C1), $LP_1(X)$, $\sigma_{C1\text{-}X}$, and $\sigma^*_{C1\text{-}X}$ NLMO contributions (Figure 5b and 5d). The fact that only a few orbitals are responsible for the observed trends simplifies the analysis considerably.

In the calculations where SO coupling is included variationally in the ground state calculation, the $\sigma^*_{C1\text{-}X}$ NLMO serves a dual role. As explained in Section 2, the shielding analysis of the SO calculation is carried out in the full set of SR NLMOs. In the SR calculations, the NLMOs have occupations of 2 or 0. Small changes of the ground state in the presence of SO coupling cause small changes in these occupations leading to an explicit shielding contribution from the $\sigma^*_{C1\text{-}X}$ NLMO in the analysis. The same NLMO also implicitly contributes to the shielding if it is important in describing the response of the molecule to the magnetic field. In the discussion of the paramagnetic shielding, we invoke the unoccupied SR orbitals in the latter sense, i.e. their

role in describing the magnetic field response.

$LP_{1,3}(X)$ contributions are taken into account in σ^{para} of Figure 5, because they contribute ca. -8 ppm to the large negative values when X = F relative to benzene. However, only a small change along the series F – I is observed (Figure S1). Therefore, in order to understand the main trends highlighted in sub-section 3.1, $\pi_{C\text{-}C}$ and $\sigma_{C1\text{-}C,X}$ orbital contributions to σ^{para} are discussed separately in the following two sub-sections. Orbital contributions to σ^{SO} are investigated subsequently.

3.4 $\pi_{C\text{-}C}$ orbital contributions to the paramagnetic C1 shielding

Figure 6 shows the σ^{para} trends obtained from the combined shielding contributions from the three doubly occupied $\pi_{C\text{-}C}$ NLMOs. As it is typical for aryl compounds, the ring π NLMOs are strongly delocalized (an example is shown in Figure 7a). Not unexpectedly, the L (Lewis) component is the main contribution for the $\pi_{C\text{-}C}$ NLMO centered on the C1–C2 bond, while the NL (non-Lewis) component is important for the other two π orbitals, due to the delocalization onto C1.

Figure 6 shows that the $\pi_{C\text{-}C}$ NLMO contributions to the C1 shielding are strongly affected by the presence of the fluorine atom, producing a sizable de-shielding. Moreover, a significant decrease of the magnitude of the negative $\pi_{C\text{-}C}$ NLMO contributions is observed along the series from F to I, which augments the NHD caused by the SO coupling.

The trend along the X series is described by the in-plane σ_{22} shielding component (Fig. S2) of C1 σ^{para}, which is perpendicular to the C1–X direction. Large negative contributions are obtained for F, while for X = I they are positive. The Cl and Br derivatives show intermediate values between F and I. The trends for the other two tensor components (σ_{11} and σ_{33}) are weak and not

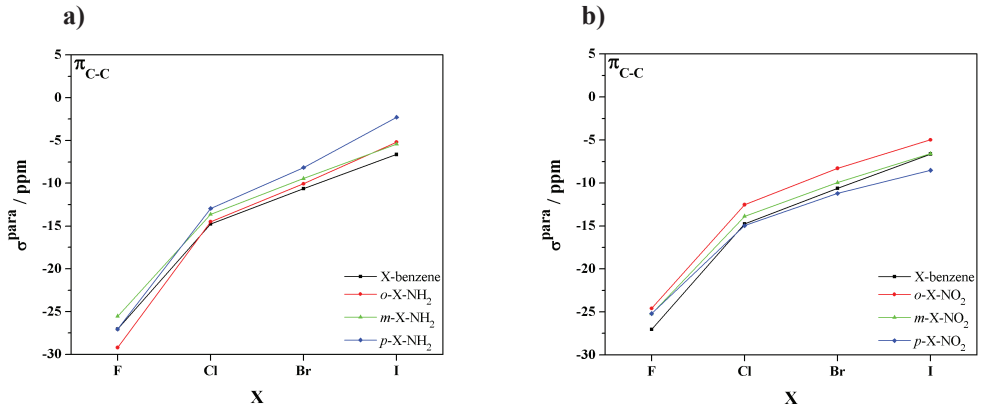

Figure 6: $\pi_{C\text{-}C}$ NLMO contributions to the isotropic σ^{para} term of the C1 shielding for X-benzenes, X-NH_2-benzenes **(a)**, and X-NO_2- benzenes **(b)** (in ppm). Each value refers to the sum of contributions from three $\pi_{C\text{-}C}$ orbitals.

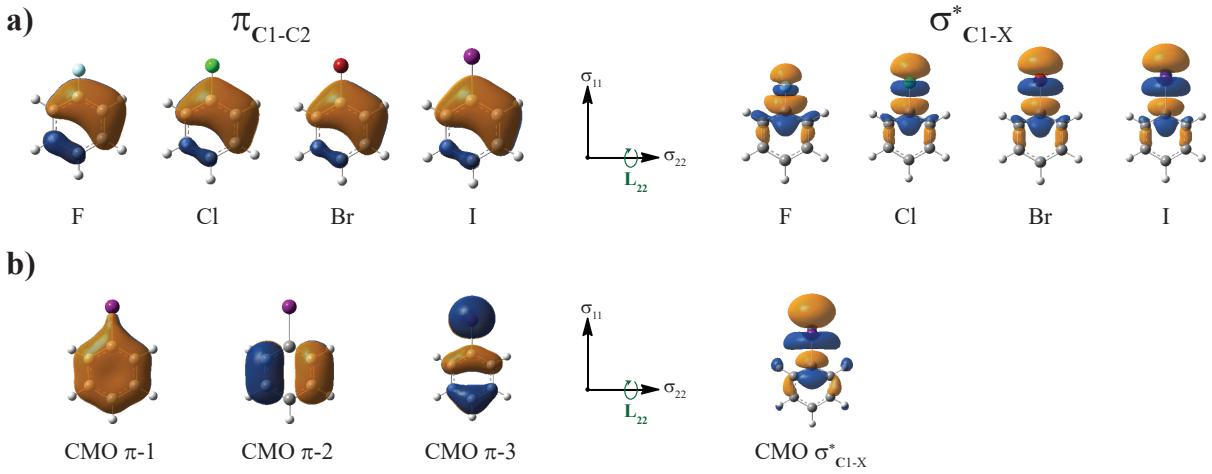

Figure 7: Isosurfaces (±0.03 au) of π_{C1-C2} NLMOs (**a**) and π_{C-C} CMOs (**b**) that may rotate under the action of the angular momentum operator (L) in σ_{22} and show symmetry with σ^*_{C1-X} unoccupied orbitals.

responsible for the overall observed shift trends.

As illustrated in Figure 7, an orbital rotation around the σ_{22} axis, representing a perturbation by the magnetic field in this direction, rotates the C1-centered part of the π_{C-C} orbital into the ring plane, which creates overlap with the σ^*_{C1-X} unoccupied orbitals. Since there is a strong a dependence of the π_{C-C} NLMO shielding contributions on the X atom, it makes sense that the dominant matrix elements in eq. (3) should depend on the σ^*_{C1-X} orbitals.

In the NBO analysis, the X-benzene σ^*_{C1-F} antibonding orbital has 71% of its density on C1, and approximately 55%, 53%, and 47% when X = Cl, Br and I, respectively. Numerical data can be found in Table S16, but the trend is readily visible in Figure 7. This trend is expected because in the corresponding σ_{C1-X} *bonding* set, the orbital is polarized strongly toward F, owing to its electronegativity, and less so for Cl, Br, and I. The C–X bonds for X = Cl, Br, I have a quite even distribution over the two atoms, which is consequently reflected also in the corresponding antibonding orbitals.

Therefore, the magnetic-field induced rotated-$\pi_{C-C} - \sigma^*_{C1-X}$ overlap at the C1 atom is strongest in the fluorine compounds. The reader is reminded that the OP interaction (Eq. 3) depends as r^{-2} on the electron-nucleus distance, i.e., the overlap right around C1 dominates the paramagnetic shielding mechanism and explains the strong de-shielding from the π NLMOs when X = F. The σ_{22} shielding contributions become less negative / more positive from X = F to I, which is likewise explained qualitatively by the decreasing density of σ^*_{C1-X} on C1. It is important to keep in mind that the C1 percentage is not the only difference between the compounds. For example, for the C–F bond the NBO analysis produces a p-rich bonding sp hybrid on F, and for the heavier halogens the

bonding orbital on X is essentially one of the valence p orbitals. Nonetheless, the orbital rotation model provides a good qualitative explanation for the plots in Figure 6.

For the small, highly symmetric X-benzene systems and the substituted derivatives, it is also illustrative to compare the localized MO analysis of the paramagnetic shielding with an analysis in terms of CMOs. CMOs with π symmetry show important contributions to the σ_{22} C1 shielding component from magnetic coupling with vacant CMOs containing features resembling the $\sigma^*_{\text{C1-X}}$ localized orbital. The three $\pi_{\text{C-C}}$ CMOs (π-1, π-2, π-3) and one such unoccupied CMO of iodobenzene are displayed in Fig. 7b. The corresponding sums of shielding contributions are collected in Table 1 for the different halogenated compounds.

Table 1: Sum of three occupied π-CMO contributions[a] to the σ_{22} component of the σ_{para} term associated with $\pi_{\text{C-C}} - \sigma^*_{\text{C1-X}}$ interactions for X-R-benzenes.

	R						
X	H	*o*-NH_2	*m*-NH_2	*p*-NH_2	*o*-NO_2	*m*-NO_2	*p*-NO_2
F	-51.25	-63.26	-39.01	-39.36	-49.20	-47.39	-44.60
Cl	-30.53	-27.66	-16.18	-22.60	-27.57	-24.24	-25.76
Br	-3.95	-5.68	11.33	-1.39	-1.42	3.15	0.56
I	38.05	37.51	44.05	40.73	33.13	37.34	31.98

[a] The orbitals are shown in Figure 7b. The shielding contributions include terms from all vacant CMOs.

The CMO contributions follow the NLMO trends in the sense that a less negative / more positive shielding is obtained across the halogen series. The lowest energy π CMO (π-1) gives negative contributions to the σ^{para} for all halogens. The other two π CMOs (π-2 and π-3) are responsible for the X series trend (see Table S17), with contributions going from negative for F to positive for Cl, Br, and I. The sign change is not easy to rationalize because there are several vacant CMOs that contribute. Once positive, the increase from Cl to I can be tied to the reduction of the energy gap between the relevant occupied π CMOs and the lowest CMO with $\sigma^*_{\text{C1-X}}$ character (Tables S18 and S19) per Equation (3).

Clearly, the $\pi_{\text{C-C}}$ orbitals play an essential role for the X series, describing the large deshielding of fluorinated compounds as well as an increasing shielding along the series F, Cl, Br, I. Moreover, the magnetic coupling between $\pi_{\text{C-C}}$ and $\sigma^*_{\text{C1-X}}$ orbitals shows that paramagnetic currents are induced by a magnetic field when an sp^2 carbon is σ-bonded to an electronegative atom. Likely, this is also an important shielding mechanism for other, similar, systems.

The $\pi_{\text{C-C}}$ orbital contributions describe the σ^{para} variations along the X series and show minor variations with the substituents R. However, the dominant shielding effects from the R substituents are not associated with the π orbitals. This result is in keeping with our previous findings for R-

benzenes.[8]

3.5 $\sigma_{C1\text{-}C,X}$ orbital contributions to the paramagnetic C1 shielding

Combined σ^{para} contributions from $\sigma_{C1\text{-}C2}$, $\sigma_{C1\text{-}C6}$, and $\sigma_{C1\text{-}X}$ NLMOs are displayed in Figure 8. Individual contributions from these NLMOs are shown in Figure S3.

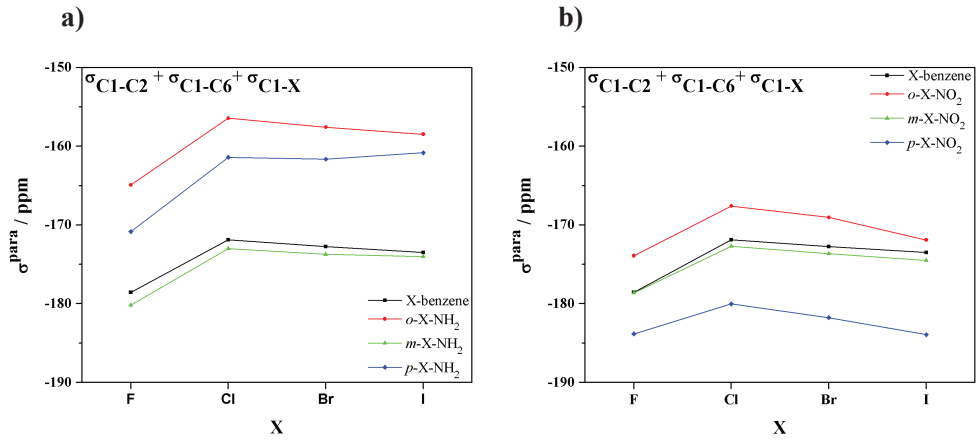

Figure 8: Sum of $\sigma_{C1\text{-}C2}$, $\sigma_{C1\text{-}C6}$, and $\sigma_{C1\text{-}X}$ NLMO contributions to the isotropic σ^{para} term of the C1 shielding for X-benzenes, X-NH_2-benzenes **(a)**, and X-NO_2-benzenes **(b)** (in ppm).

The effects due to different X are weaker for the σ orbitals than they are for the π orbitals discussed in Section 3.4. There is, however, a noticeable de-shielding 'dip' in the curves in Figure 8 for X = F. Regarding the R groups, a comparison of Figure 8 with Figure 4, center column, shows that the substituent position effects are satisfactorily described by only this set of σ orbitals for both the NH_2 and the NO_2 group, and their contributions to the paramagnetic mechanism.

Both the X and R series trends due to the σ-bonding LMOs are associated with the magnetic field pointing along the in-plane principal shielding axes (σ_{11} and σ_{22}, Fig. S4) and dominated by the Lewis parts of the NLMOs, which is expected for the weakly delocalized σ orbital framework. The σ_{11} component is associated with the $\sigma_{C1\text{-}C}$ NLMOs, while σ_{22} is mainly due to the $\sigma_{C1\text{-}X}$ NLMO. The two sets of orbitals / shielding tensor components display pronounced dependencies on the X substituent, but of opposite signs. When added, mainly only the large difference between X = F vs. X = Cl, respectively, shows up as the aforementioned 'dip' in Figure 8 but the overall trend is weak. This result shows that the electronegativity of the X atom plays a more important role for the $\pi_{C\text{-}C} - \sigma^*_{C1\text{-}X}$ magnetic coupling than for the shielding contribution from $\sigma_{C1\text{-}C,X}$.

As we noted recently for benzene, aniline and nitrobenzene,[8] a $\sigma_{C1\text{-}C,X}$ rotation around the σ_{11} and σ_{22} axes produces transformed NLMOs that overlap effectively with the same $\pi^*_{C1\text{-}C2}$ unoccupied orbital, resulting in important contributions to the σ^{para} term from different magnetic field

directions (Fig. 1). We found little numerical evidence that would unabiguously rationalize the X-dependency for the $\sigma_{C1\text{-}C}$ contributions in Figure S4. The $\sigma_{C1\text{-}C}$ show a weak dependence of their delocalization on the X substituent (Table S21), with the most localized orbitals for X = F, which may increase the overlap with $\pi^*_{C1\text{-}C2}$ upon the magnetic field interaction, leading to the most negative σ^{para} contribution. For the $\sigma_{C1\text{-}X}$ contributions, we already noted the strong changes of the orbitals' weight on C1, depending on the X substituent. The X-trend for the $\sigma_{C1\text{-}X}$ contribution in Figure S4 is essentially a reflection of the C1 weight in the orbital (Table S22).

To analyze the effect of the R substituents on the σ system of the X-benzenes, the electron density rearrangement caused by the R-substitution was investigated. Section 5 of the SI (Fig. S5 and S6) displays the σ contributions of ΔVDD atomic charges for NH_2- and NO_2-X-benzene calculated in relation to X-phenyl and substituent fragments ($\Delta VDD = VDD_{X\text{-}R\text{-}benzene} - VDD_{fragments}$). Density rearrangements in the σ systems of X-R-benzene compounds follow the trends observed for R-benzenes (see ref. 8 for details), namely they are opposite to the density rearrangements in the occupied π orbitals. While the NH_2 group causes a depletion of σ electron density on carbon atoms at *ortho* and *para* positions, an accumulation takes place at the same positions in NO_2-benzene. Carbon atoms in the *meta* positions are essentially unaffected by the R-substitutions. These electronic rearrangements are tied to changing weights of the σ orbitals on a given carbon, which lead to substantial variations of the magnetic coupling $\sigma_{C1\text{-}C,X} - \pi^*_{C1\text{-}C2}$ shown in Figure 1. An accumulation of σ electron density on C1 increases the magnitude of the negative paramagnetic contribution to the shielding, while a depletion tends to decrease the magnitude of this magnetic interaction. This mechanism is responsible for the increased shielding effect caused by the NH_2 group at *ortho* and *para* positions and the deshielding effect in *para* position when $R = NO_2$. We noted already in Reference 8 that in the $\sigma_{C1\text{-}C,X} - \pi^*_{C1\text{-}C2}$ magnetic coupling there is a reinforcing effect from the R-substituent effects on $\pi^*_{C1\text{-}C2}$: If the presence of the substituent causes the weight of the occupied $\pi_{C1\text{-}C2}$ to shift toward or away from C1, the trend in $\pi^*_{C1\text{-}C2}$ is also opposite and boosts the net effect in the σ framework.

The effect of the NO_2 substituent on the C1 shielding in *ortho* position can be rationalized by two factors: (1) the inductive polarization of the $\sigma_{C1\text{-}C2}$ bond and (2) the torsion of the NO_2 group with respect to the ring plane due to steric hindrance between NO_2 and X. The first effect was explained for X = H in Ref. 8. The X-R-benzene compounds show the same inductive polarization effects and therefore we skip the details here. In a nutshell, even though there is a net increase of σ electron density on C1 for NO_2 in *ortho* position relative to benzene from the sum of all $\sigma_{C1\text{-}C,X}$ orbitals, the strong inductive polarization decreases the C1 weight in the $\sigma_{C1\text{-}C2}$ orbital. The weakened magnetic coupling of this orbital in the σ^{para} mechanism is responsible for an increased *ortho*-C1 shielding relative to benzene (Tab. S24 and Fig. S7).

The out-of-plane torsion of the NO_2 group decreases the π conjugation with the phenyl ring,

and therefore the mirror-image patterned σ deformation densities displayed by the completely planar geometry in Figures S5 and S6 may become less pronounced, with concomitant effects on the paramagnetic shielding contribution. In order to verify this hypothesis, the C1 shielding tensor was calculated upon changing the C_1-C_2-N-O dihedral angle (θ) in 10°steps, from 0°to 90°. The geometries were optimized allowing all other geometrical parameters to relax (PBE0/TZ2P). σ^{para} data *versus* the dihedral angle are displayed in Figure S8 for the *o*-X-NO_2-benzenes.

The torsion is important for X = Cl, Br, and I since the steric hindrance becomes large for these compounds. Consequently, the equilibrium angle (∼40°) is far from planar. The reduction of the magnitude of σ^{para} caused by the torsion is about 4-5 ppm for the Cl, Br, and I derivatives, but does not explain the effect for fluorine derivatives. For X = F, only the polarization effect of the $\sigma_{\text{C1-C2}}$ bond is present.

3.6 Orbital contributions to the SO shielding

Regarding the σ^{SO} term, this shielding mechanism represents an interplay between the SO coupling at the Heavy Atom (HA) and the spin-dependent Fermi contact (FC) and spin-dipolar (SD) nuclear hyperfine mechanisms at the Light Atom (LA). The SO/FC mechanism is usually considered as the most important transmission mechanism to explain the HA effect on the ^{13}C NMR shielding tensor. This mechanism is associated with a transmission of magnetic field-induced spin polarization through a covalent bond from the HA to a neighboring LA nucleus.[11,14] This mechanism is most effective when the LA atomic hybrids forming the bond have considerable s character, because spin polarization of valence s orbitals directly creates spin density at the nucleus where it is 'detected' by the FC mechanism.

For the studied molecules, the σ^{SO} term is essentially described by four orbital contributions displayed in Fig.5b and Fig. 5d. CR (C1), LP_1(X), and the $\sigma_{\text{C1-X}}$ and $\sigma^*_{\text{C1-X}}$ NLMO contributions represent more than 80% of the total σ^{SO} term. These orbital contributions increase along the X series (NHD behavior), indicating that the SO shielding effect is associated with orbitals from the carbon 1s shell, an in-plane s-rich halogen lone pair, and valence $\sigma_{\text{C1-X}}$ orbitals. A contribution from the $\sigma^*_{\text{C1-X}}$ NLMO in the shielding analysis arises because unoccupied orbitals of the spin-free system describe the SO effects on the ground state electronic structure, as already mentioned.

As already mentioned, σ^{SO} shows for the X-NH_2-benzenes an inversion of the substitution effect between *ortho* and *para* isomers when going from X = Cl to I, mainly die to a smaller σ^{SO} when the NH_2 group is in *ortho* position. The LP_1(X) contributions do not show important differences among the position isomers. Thus, the effect of the NH_2 group on σ_{SO} is governed by the NLMO contributions listed in Table 2. The listed NLMO contributions to σ^{SO} increase universally along the series X = F, Cl, Br, I, but less strongly so for the *ortho* isomer. For the

Table 2: CR (C1), $\sigma_{\text{C1-X}}$, and $\sigma^{*}_{\text{C1-X}}$ contributions to the σ^{SO} term of the C1 shielding for X-NH_2-benzenes (in ppm).

	CR (C1)				$\sigma_{\text{C1-X}}$				$\sigma^{*}_{\text{C1-X}}$			
X	H	*o*-NH_2	*m*-NH_2	*p*-NH_2	H	*o*-NH_2	*m*-NH_2	*p*-NH_2	H	*o*-NH_2	*m*-NH_2	*p*-NH_2
F	0.88	0.88	0.87	0.85	0.07	0.06	0.07	0.06	0.20	0.19	0.19	0.19
Cl	1.54	1.44	1.50	1.49	0.49	0.44	0.47	0.48	1.24	1.10	1.19	1.16
Br	6.02	5.35	5.97	6.12	1.35	2.94	3.15	3.26	5.35	4.67	5.25	5.22
I	15.59	13.58	15.37	15.74	9.56	8.56	9.24	9.65	11.58	9.53	10.94	11.20

$\sigma_{\text{C1-X}}$ NLMO (Table 3), the weight of C1 is the smallest for *o*-X-NH_2-benzene compared to X-benzene and the *meta* and *para* R-substituted derivatives. Therefore, the proximity of the NH_2 group in the *ortho* isomer causes a slight reduction of the σ electron density on C1, which renders the contribution to σ^{SO} from the $\sigma_{\text{C1-X}}$ less effective. The variations among the C1 core orbitals are too small to give any insight into the CR(C1) trend in Table 3. The variations in this orbital's contribution to the C1 shielding, however, must ultimately be coupled to the valence shell trends and their influence on high-energy virtual orbitals with large C1 character, similar to core orbital contributions to NMR J-coupling.[39] We therefore assign the less effective SO effect from X in the presence of the *ortho*-NH_2 group mainly to an inductive mechanism. For the NO_2 group, while the inductive effect on $\sigma_{\text{C1-C2}}$ is very strong in *ortho position*, as mentioned above, the combined effects on this and the other σ orbitals render the SO effect on the C1 shielding slightly larger for *ortho*-NO_2 compared to the other positions. This finding highlights the complications of analyzing strong effects on one orbital in a self-consistent set of orbitals.

4 Conclusions

This study has investigated the effects of X (F, Cl, Br, I) and R (NH_2 and NO_2) groups on ^{13}C NMR chemical shifts in X-R-benzenes. As observed previously by us for R-benzenes,[8] the σ orbitals ($\sigma_{\text{C1-C2}}$, $\sigma_{\text{C1-C6}}$, and $\sigma_{\text{C1-X}}$) are identified as the main source for the shielding/de-shielding effects

Table 3: Atomic hybrid contributions of the C1 (%C1) to $\sigma_{\text{C1-X}}$ NLMO for X-NH_2-benzenes.

	$\sigma_{\text{C1-X}}$			
X	H	*o*-NH_2	*m*-NH_2	*p*-NH_2
F	28.07	27.99	27.96	28.08
Cl	43.36	43.01	43.14	43.23
Br	46.10	45.64	45.84	45.92
I	51.70	51.08	51.42	51.45

of the R groups depending on their position relative to C1. The present analysis shows that these findings translate to the X-R-benzenes even though the polarization of the C–X σ bond strongly varies with X.

The π system is important to describe the X effects in the paramagnetic shielding tensor mechanism. Despite the halogens, specially F, showing an electron-withdrawing inductive effect from the carbon only in the σ system, the occupied π orbitals are responsible for the paramagnetic shielding trends along the X series. This happens because the paramagnetic shielding trend in the series comes from the magnetic coupling between occupied $\pi_{\text{C-C}}$ and unoccupied $\sigma^*_{\text{C1-X}}$ orbitals, and the polarization of the latter strongly determines the magnitude of the coupling. In turn, the $\sigma^*_{\text{C1-X}}$ polarization depends on the polarization of the occupied $\sigma_{\text{C1-X}}$, which is driven by the inductive effect of X.

X and R groups also show effects on the σ^{SO} component of the C1 shielding tensor. An NHD behavior is observed along the X series and mainly caused by the SO effects from occupied and unoccupied $\sigma_{\text{C1-X}}$ orbitals. The R groups affect the intensity of the NHD trend mainly only when NH_2 is in *ortho* position, which can be assigned to an inductive effect that renders the magnetic field-induced spin polarization on C1 less effective. When the inductive effect is even stronger, as with *ortho*-NO_2, however, the coupled response from multiple σ orbitals more or less cancels in the X-dependence of σ^{SO}.

The results displayed in this work show that X and R effects on the chemical shift in benzene systems can be understood as mainly additive, since the shielding trends for each group are predominantly described by orbitals with different symmetries. While the X effect is explained by the magnetic coupling involving π orbitals, σ orbitals describe the trends caused by R groups. A synergy among those effects is only evident in the σ^{SO} term when X and NH_2 groups are in an *ortho* arrangement.

Acknowledgments

We acknowledge FAPESP for financial support (2011/17357-3, 2013/03477-2, 2015/08541-6, and 2017/17750-3), scholarships to R. V. V. (2012/12414-1, 2015/20106-3, and 2017/20890-1) and a fellowship to L. C. D. (2014/21930-9). We are grateful for fellowships from CNPq to C. F. T. and L. C. D. (202068/2015-3). J. A. acknowledges National Science Foundation (grant CHE-1560881) for financial support. The authors thank the Center for Computational Research (CCR) at the University at Buffalo for providing computational resources. Thanks are extended to Dr. Célia Fonseca Guerra for providing information about the VDD analysis in ADF.

Supporting information available

Experimental ^{13}C NMR chemical shifts, DFT benchmark for chemical shift calculations, individual components of the ^{13}C NMR shielding tensor, lists and graphics of NLMO contributions, and tables of NLMO properties.

References

[1] M. H. Levitt, *Spin dynamics: Basics of nuclear magnetic resonance 2nd ed.*, John Wiley & Sons, Chichester, 2008.

[2] L. J. Mueller, *Concepts in Magn. Reson. Part A*, 2011, **38A**, 221–235.

[3] N. E. Jacobsen, *NMR Spectroscopy Explained: Simplified Theory, Applications and Examples for Organic Chemistry and Structural Biology*, John Wiley & Sons, Hoboken, USA, 2007.

[4] J. H. Simpson, *Organic Structure Determination Using 2-D NMR Spectroscopy*, Elsevier, Burlington, 2008.

[5] J. Clayden, N. Greevs, S. Warren, P. Wothers, *Organic Chemistry 1st ed.*, Oxford University Press, New York, 2000.

[6] S. E. Wheeler, K. N. Houk, *J. Am. Chem. Soc.*, 2009, **131**, 3126–3127.

[7] J. W. Bloom, R. K. Raju, S. E. Wheeler, *J. Comput. Chem.*, 2012, **8**, 3167–3174.

[8] R. V. Viesser, L. C. Ducati, C. F. Tormena, J. Autschbach, *Chem. Sci.*, 2017, **8**, 6570–6576.

[9] J. B. Grutzner in *Recent advances in organic NMR spectroscopy*, Norell Press, Landisville, NJ, 1987, pp. 17–42.

[10] R. G. Kidd, *Annu. Rep. NMR Spectrosc.*, 1980, **10A**, 1.

[11] M. Kaupp, O. L. Malkina, V. G. Malkin, P. Pyykkö, *Chem. Eur. J.*, 1998, **4**, 118–126.

[12] Y. Nomura, Y. Takeuchi, N. Nakagawa, *Tetrahedron Lett.*, 1969, **8**, 639–642.

[13] I. Morishima, K. Endo, T. Yonezawa, *J. Chem. Phys.*, 1973, **59**, 3356–3364.

[14] J. Autschbach in *High Resolution Nuclear Magnetic Resonance Parameters for Understanding Molecules and their Electronic Structure*, Vol. 3 of *Science & Technology of Atomic, Molecular, Condensed Matter & Biological Systems*, R. H. Contreras (Ed.), Elsevier, Amsterdam, 2013, pp. 69–117.

[15] J. Autschbach, S. Zheng, *Annu. Rep. NMR Spectrosc.*, 2009, **67**, 1–95.

[16] H. Nakatsuji, Z.-M. Hu, T. Nakajima, *Chem. Phys. Lett.*, 1997, **275**, 429–436.

[17] E. J. Baerends, T. Ziegler, J. Autschbach, D. Bashford, A. Bérces, F. M. Bickelhaupt, C. Bo, P. M. Boerrigter, L. Cavallo, D. P. Chong, L. Deng, R. M. Dickson, D. E. Ellis, M. van Faassen, L. Fan, T. H. Fischer, C. Fonseca Guerra, A. Ghysels, A. Giammona, S. J. A. van Gisbergen, A. W. Götz, J. A. Groeneveld, O. V. Gritsenko, M. Grüning, S. Gusarov, F. E. Harris, P. van den Hoek, C. R. Jacob, H. Jacobsen, L. Jensen, J. W. Kaminski, G. van Kessel, F. Kootstra, A. Kovalenko, M. V. Krykunov, E. van Lenthe, D. A. McCormack, A. Michalak, M. Mitoraj, J. Neugebauer, V. P. Nicu, L. Noodleman, V. P. Osinga, S. Patchkovskii, P. H. T. Philipsen, D. Post, C. C. Pye, W. Ravenek, J. I. Rodríguez, P. Ros, P. R. T. Schipper, G. Schreckenbach, J. S. Seldenthuis, M. Seth, J. G. Snijders, M. Solà, M. Swart, D. Swerhone, G. te Velde, P. Vernooijs, L. Versluis, L. Visscher, O. Visser, F. Wang, T. A. Wesolowski, E. M. van Wezenbeek, G. Wiesenekker, S. K. Wolff, T. K. Woo, A. L. Yakovlev, *Amsterdam Density Functional, SCM, Theoretical Chemistry, Vrije Universiteit, Amsterdam, The Netherlands.*, URL `https://www.scm.com`. Accessed 03/17. `https://www.scm.com`.

[18] G. te Velde, F. M. Bickelhaupt, E. J. Baerends, S. J. A. van Gisbergen, C. Fonseca Guerra, J. G. Snijders, T. Ziegler, *J. Comput. Chem.*, 2001, **22**, 931–967.

[19] C. Fonseca Guerra, J. G. Snijders, G. te Velde, E. J. Baerends, *Theor. Chem. Acc.*, 1998, **99**, 391.

[20] C. Adamo, V. Barone, *J. Chem. Phys.*, 1999, **110**, 6158–6170.

[21] M. Franchini, P. H. T. Philipsen, L. Visscher, *J. Comput. Chem.*, 2013, **34**, 1819–1827.

[22] A. Klamt, G. Schüürmann, *J. Chem. Soc. Perkin Trans. 2*, 1993, 799–805.

[23] E. van Lenthe, E. J. Baerends, J. G. Snijders, *J. Chem. Phys.*, 1993, **99**, 4597–4610.

[24] E. van Lenthe, A. Ehlers, E. J. Baerends, *J. Chem. Phys.*, 1999, **110**, 8943–8953.

[25] S. K. Wolff, T. Ziegler, E. van Lenthe, E. J. Baerends, *J. Chem. Phys.*, 1999, **110**, 7689–7698.

[26] J. Autschbach, E. Zurek, *J. Phys. Chem. A*, 2003, **107**, 4967–4972.

[27] J. Autschbach, *Mol. Phys.*, 2013, **111**, 2544–2554.

[28] A. Greif, P. Hrobarik, A. Arbuznikov, J. Autschbach, M. Kaupp, *Inorg. Chem.*, 2015, **54**, 7199–7208.

[29] A. Greif, P. Hrobarik, J. Autschbach, M. Kaupp, *Phys. Chem. Chem. Phys.*, 2016, **18**, 30462–30474.

[30] E. D. Glendening, C. R. Landis, F. Weinhold, *J. Comput. Chem.*, 2013, **34**, 1429–1437.

[31] J. Autschbach, S. Zheng, *Magn. Reson. Chem.*, 2008, **46**, S48–S55.

[32] J. Autschbach, *J. Chem. Phys.*, 2008, **128**, 164112.

[33] K. Sutter, G. A. Aucar, J. Autschbach, *Chem. Eur. J.*, 2015, **21**, 18138–18155.

[34] S. Moncho, J. Autschbach, *Magn. Reson. Chem.*, 2010, **48**, S76–85.

[35] O. A. Stasyuk, H. Szatylowicz, T. M. Krygowski, C. Fonseca Guerra, *Phys. Chem. Chem. Phys.*, 2016, **18**, 11624–11633.

[36] C. Fonseca Guerra, J.-W. Handgraaf, E. J. Baerends, F. M. Bickelhaupt, *J. Comput. Chem.*, 2004, **25**, 189–210.

[37] L. Guillaumes, S. Simon, C. Fonseca Guerra, *ChemistryOpen*, 2015, **4**, 318–327.

[38] J. Toušek, M. Straka, V. Sklenář, R. Marek, *J. Phys Chem. A*, 2013, **117**, 661–669.

[39] J. Autschbach, B. Le Guennic, *J. Chem. Educ.*, 2007, **84**, 156–171.

Table of Contents

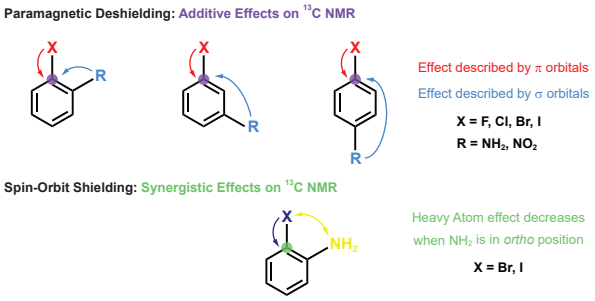

X (F, Cl, Br, I) and R (NH_2, NO_2) group effects on ^{13}C NMR chemical shifts are explained by π and σ orbitals, respectively.

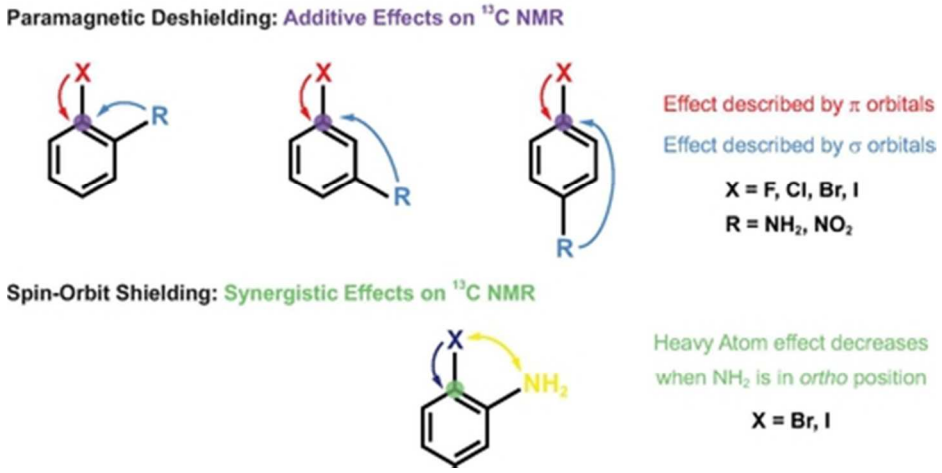

X (F, Cl, Br, I) and R (NH_2, NO_2) group effects on ^{13}C NMR chemical shifts are explained by π and σ orbitals, respectively.

39x19mm (300 x 300 DPI)